Negative Interfacial Tension in Phase-Separated Active Brownian Particles

Julian Bialké,[1] Jonathan T. Siebert,[2] Hartmut Löwen,[1] and Thomas Speck[2]
[1]Institut für Theoretische Physik II, Heinrich-Heine-Universität, D-40225 Düsseldorf, Germany
[2]Institut für Physik, Johannes Gutenberg-Universität Mainz, Staudingerweg 7-9, 55128 Mainz, Germany
(Received 15 December 2014; revised manuscript received 24 July 2015; published 24 August 2015)

We study numerically a model for active suspensions of self-propelled repulsive particles, for which a stable phase separation into a dilute and a dense phase is observed. We exploit the fact that for nonsquare boxes a stable "slab" configuration is reached, in which interfaces align with the shorter box edge. Evaluating a recent proposal for an intensive active swimming pressure, we demonstrate that the excess stress within the interface separating both phases is negative. The occurrence of a negative tension together with stable phase separation is a genuine nonequilibrium effect that is rationalized in terms of a positive stiffness, the estimate of which agrees excellently with the numerical data. Our results challenge effective thermodynamic descriptions and mappings of active Brownian particles onto passive pair potentials with attractions.

DOI: 10.1103/PhysRevLett.115.098301 PACS numbers: 82.70.Dd, 64.60.Cn

Equilibrium statistical physics [1] rests on two deceptively simple premises: The laws of conservation and the uniform probability of all accessible microstates in isolated systems. Of course, suitable local equilibria are only a small part of the Universe and nonequilibrium encompasses so many diverse processes and phenomena that the quest for a universal description is one of the great challenges in statistical physics. While likely futile in full generality, there are subclasses of driven systems for which a comprehensive theory seems to be within reach. One such class are suspensions of active particles.

Active matter [2–4] has emerged as a paradigm to describe a broad wealth of nonequilibrium collective dynamical behavior, including (but not limited to) droplets [5], bacteria [6], and microtubule networks driven by molecular motors [7]. Here we focus on active Brownian particles (ABPs), a model for self-propelled colloidal spherical particles suspended in a solvent (see Ref. [8] for a short perspective of these systems and for references) or a polymer solution [9]. Quite strikingly, particles cluster into dense and dilute regions for high-enough density and swimming speeds. Such behavior has been observed both experimentally [10–12] and in computer simulations of purely repulsive particles without [13–19] and with [20–22] hydrodynamic interactions. Microscopically, this has been understood to arise from the time-scale separation between the decorrelation time of the directed motion and the collision rate, which is controlled by speed and density. The actual time scales depend on many details (pair potentials, swimming mechanisms, and hydrodynamic interactions [22]), but the generic effect is robust and only requires volume exclusion in combination with a persistent motion of the particles.

Because the formation and growth of dense domains indeed resembles the phase separation of passive suspensions with attractive interactions, several theoretical descriptions following a "thermodynamical" route have been proposed, including effective mean-field free energies [23–25], pressure equations of state [19,26–28], and mappings to effective isotropic pair potentials [9,29]. However, microscopic pair correlations of the self-propelled particles are not isotropic and the crucial physical ingredient is the persistence of motion over a length $\ell_p = v_0\tau_r$, where v_0 is the swimming speed and τ_r the time over which orientations decorrelate.

In this Letter, we numerically test the idea of an *intensive* pressure for ABPs. To this end one has to assume an equation of state exists [30], as supported by simulations [19,28,31]. We adopt a strategy, proven to be very fruitful in the study of phase-separated passive systems, of exploiting finite-size transitions in nonsquare simulation boxes [32]. We follow old ideas by Kirkwood and Buff [33], together with a generalization of the swimming pressure [19], and thus obtain access to the interface [34]. We show that the interfacial *tension* extracted from the excess mechanical stress is actually negative. In contrast, the *stiffness* governing the interface fluctuations is positive, and we show how to relate both through the dissipated work.

We simulate a minimal model that has been studied by a number of groups [13–19]. The model consists of N particles with diameter a interacting via short-ranged repulsive forces [here from a Weeks-Chandler-Andersen potential $u(r)$, for details and parameters see Refs. [8,12]]. The dynamics is overdamped,

$$\dot{\mathbf{r}}_i = -\nabla_i U + v_0\mathbf{e}_i + \boldsymbol{\xi}_i, \tag{1}$$

where $\boldsymbol{\xi}_i$ is the Gaussian translational noise with zero mean and correlations $\langle\boldsymbol{\xi}_i(t)\boldsymbol{\xi}_j^T(t)\rangle = 2\delta_{ij}\mathbf{1}\delta(t-t')$, and $U = \sum_{j<i}u(|\mathbf{r}_i - \mathbf{r}_j|)$ is the total potential energy. We consider the two-dimensional case with a simulation box of size

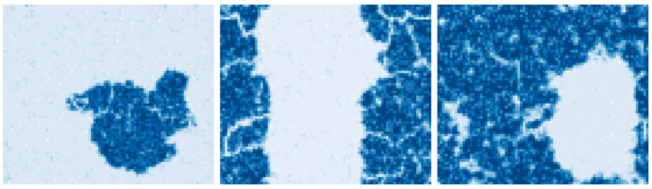

FIG. 1 (color online). Finite-size transitions of ABPs (in a box with aspect ratio 1.2) going from low to high density: Droplet ($\phi \simeq 0.30$), slab ($\phi \simeq 0.54$), and bubble ($\phi \simeq 0.74$). Density maps are shown, where cells are colored according to their local structure (the darker the color, the more highly structured the cell); see [35] for the definition of local structure.

$L_x \times L_y$ employing periodic boundary conditions. Every particle swims with fixed speed v_0 along its unity orientation $\mathbf{e}_i$, which undergoes free rotational diffusion with diffusion coefficient $1/\tau_r$. We employ dimensionless quantities such that lengths are measured in units of a and time in units of a^2/D_0, where D_0 is the bare translational diffusion coefficient. In the following we use $\tau_r = \frac{1}{3}$, which follows from the no-slip boundary condition for colloidal particles. Moreover, energies are measured in units of k_BT for fixed solvent temperature T.

We first scan the system for swimming speed $v_0 = 180$ and vary the global density $\bar{\rho} = N/A$. As shown in Fig. 1, we observe finite-size transitions as we increase the density from the homogeneous suspension to a droplet of the dense phase, then to a slab, and then to a "bubble" (or void) forming within the dense phase. These transitions appear to be exact counterparts of the transitions observed in simulations of vapor-liquid coexistence in finite volumes [40]. While the snapshots in Figs. 1, 2(a), and 2(b) show a high degree of local order in the dense phase, these crystalline patches have only a short lifetime and constantly reorganize. Hence, particles do not freeze, and the description as an active liquid-vapor coexistence is more appropriate.

To make comparisons with passive suspensions easier, densities will be reported as area fractions $\phi = \bar{\rho}\pi(a^*/2)^2$ using an effective hard-sphere diameter $a^* \simeq 0.986a$ obtained via Barker-Henderson theory from the pair potential [41]. Such a mapping is known to work well for passive repulsive suspensions, although at high swimming speeds it will certainly become less reliable. In the following, we exploit the slab configuration; all simulations are run at global area fraction $\phi = 0.5$, varying the speed v_0. In analogy to simulations of passive fluids, we employ a nonsquare box of area $A = L_xL_y$ with edge lengths $L_x > L_y$ such that the slab of the dense phase is encouraged to span the shorter length, see Fig. 2(a). At high-enough swimming speeds v_0, such slabs form spontaneously and remain stable. In order to reach the steady state faster, all N particles are initially placed in a dense slab in the middle of the system. After a relaxation time that depends on the system size N, we start to collect and analyze data.

Looking at the simulations qualitatively, one notes that fluctuations are much more violent than expected from a passive suspension. In particular, larger bubbles might form even in the dense phase, see Fig. 2(b). Still, given sufficient statistics, the averaged density profiles excellently fit the functional form

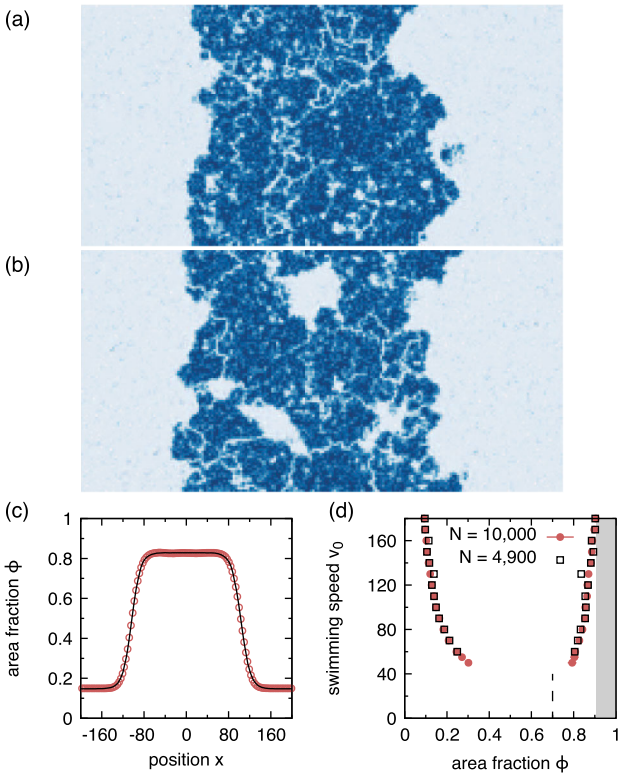

FIG. 2 (color online). Slab geometry. (a),(b) Snapshots of a phase-separated system with aspect ratio $L_x/L_y = 2$ for $N = 52386$ particles. In the steady state a dense slab is surrounded by the dilute gas phase (color code as for Fig. 1). (b) Large fluctuations occur, not only at the interface; the dense inner region of the slab might also develop "holes." (c) Measured density profile for $v_0 = 100$ (symbols) and fit of Eq. (2) (line). (d) Resulting phase diagram for two system sizes; the symbols show the coexisting densities $\phi_\pm$. The dashed vertical line indicates the freezing area fraction $\phi \simeq 0.7$, and the shaded area indicates the excluded packing fractions for real hard disks.

$$\phi(x) = \frac{\phi_+ + \phi_-}{2} + \frac{\phi_+ - \phi_-}{2}\tanh\left(\frac{x - x_0}{2w}\right), \qquad (2)$$

see Fig. 2(c). Here, x_0 marks the midpoint of the profile and w is related to the width of the interface. Density profiles are measured from the simulations by dividing the simulation box into slices with area $A_1 = A/N_b$, where x is the distance of the slice from the center of mass and N_b is the number of bins employed. Although the two interfaces are correlated, in a first attempt we treat them independently and perform separate fits for $x < 0$ and $x > 0$. The interfacial width w and bulk phase densities $\phi_\pm$ are then obtained by taking the mean of the results for the left and right half of the box. We fit Eq. (2) for each profile, from

which we extract the coexisting densities $\phi_\pm$ shown in Fig. 2(d). No systematic finite-size effects for the coexisting densities seem to be present for speeds $v_0 \gtrsim 60$ for the system sizes N studied here.

We now study the mechanical stress in more detail. To this end, we focus on the single swimming speed $v_0 = 100$. Note that the system is translationally invariant in the y direction because we have encouraged the slab to align that way. Clearly, phase separation and the occurrence of interfaces break the translational invariance in the x direction so that averaged quantities can depend only on x.

We first consider the pressure tensor

$$p^{(i)}(x) = \frac{1}{2A_1}\langle \mathbf{r}_{ij}\mathbf{f}^T_{ij}\rangle_x \tag{3}$$

due to particle interactions, where $\mathbf{r}_{ij} = \mathbf{r}_i - \mathbf{r}_j$ is the connecting vector of particles i and j, and $\mathbf{f}_{ij}$ is the pair force along this vector due to the repulsive potential. The brackets $\langle\cdot\rangle_x$ denote the average over particle pairs for which at least one particle is within the slice at x. The factor $\frac{1}{2}$ has to be included to compensate for the fact that every bond crossing between slices is counted twice. Note that there are alternative spatial discretization schemes, all of which lead to the same integrated pressure [42]. The two diagonal components $p^{(i)}_{xx}$ and $p^{(i)}_{yy}$ are plotted in Fig. 3(a). Both curves lie on top of each other and qualitatively follow the density; i.e., the interaction pressure is low in the dilute phase and high in the dense phase. Clearly, there is something missing, because such an inhomogeneous pressure would lead to an unstable system. Generally, the divergence $\nabla\cdot\mathbf{p}$ of the total mechanical stress $\mathbf{p}(\mathbf{r})$ is related to the force on an area element at $\mathbf{r}$. From the absence of a particle current

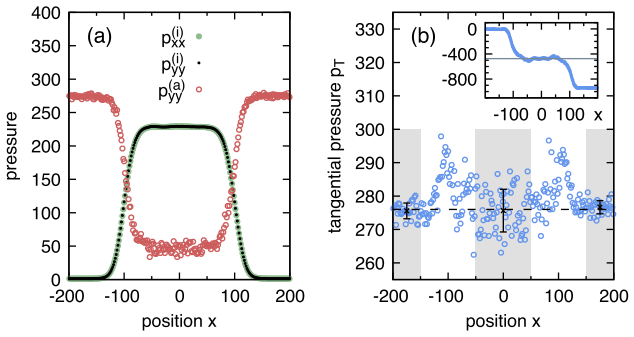

FIG. 3 (color online). Pressure profiles for $v_0 = 100$ and $N = 52386$. (a) The diagonal components $p^{(i)}_{xx}$ (filled circle) and $p^{(i)}_{yy}$ (dot) of the interaction pressure (which lie on top of each other) and the tangential active pressure $p^{(a)}_{yy}$ (open circle). (b) The total tangential pressure $p_T = \rho + p^{(i)}_{yy} + p^{(a)}_{yy}$. The dashed horizontal line is the estimate for the bulk pressure $p \simeq 276$. The error bars show the root-mean-square errors of local fits within the shaded areas corresponding to the dilute (outer) and dense (inner) phase. In the inset the symmetrized integral of the pressure difference $p - p_T$ is plotted, where the vertical line shows the estimated value $\gamma \simeq -475$ for the interfacial tension.

for ABPs one can thus conclude that $\nabla\cdot\mathbf{p} = 0$, which is the condition for hydrostatic equilibrium (a more involved calculation is presented in Ref. [43]). This condition implies that the tensor $\mathbf{p}(x)$ is diagonal and, moreover, that the normal pressure $p_{xx} = p_N$ is constant throughout the box. In contrast, the tangential pressure $p_{yy}(x) = p_T(x)$ can, and does, vary spatially with x.

The idea has been formalized only very recently that, due to their directed motion, the particles exert a mechanical stress [19,31] leading to a scalar active pressure

$$p^{(a)} = \frac{v_0}{2A}\sum_{i=1}^{N}\langle \mathbf{e}_i\cdot\mathbf{r}_i\rangle, \tag{4}$$

where $\mathbf{r}_i$ is indeed the absolute position. The active pressure thus stems from the correlations between particle positions and orientations. Assuming a gas of noninteracting swimmers with $\dot{\mathbf{r}}_i = v_0\mathbf{e}_i + \boldsymbol{\xi}_i$, we obtain the ideal active pressure [19]

$$p^{(a)}_{\mathrm{id}} = \frac{v_0}{2A}\sum_{i=1}^{N}\int_{-\infty}^{t} dt'\langle \mathbf{e}_i(t)\cdot\dot{\mathbf{r}}_i(t')\rangle = \frac{1}{2}\bar{\rho}v_0^2\tau_r \tag{5}$$

using the correlation function $\langle \mathbf{e}(t)\cdot\mathbf{e}(t')\rangle = e^{-|t-t'|/\tau_r}$.

To consider the spatial dependence of the active pressure (4), we introduce the generalized tensor

$$\mathbf{p}^{(a)}(x) = \frac{v_0}{A_1}\langle \mathbf{e}_i\mathbf{r}_i^T\rangle_x \tag{6}$$

in analogy to Eq. (3). The time average is now taken for the subset of particles that at time t occupy slice x. However, there is a subtlety here, since this destroys the correlations between the x coordinate and the orientations, which, as Eq. (5) demonstrates, depend not only on the configuration but on the previous history. Hence, only the component $p^{(a)}_{yy}(x)$, which is plotted in Fig. 3(a), is actually meaningful. This component again qualitatively follows the density, but is now inverted with respect to the interaction pressure: The active pressure is high in the dilute region and drops considerably in the dense region. The physical reason for this is that particle motion is hindered in the dense phase; orientation and actual displacement are thus less correlated.

While the fitted coexisting densities seem to have converged, we found that the active pressure is much more sensitive to system size. We thus study an even larger system with $N = 52386$ particles, the results for which are shown in Fig. 3. Two conceptual insights into the nature of ABPs are gained by plotting the total tangential pressure $p_T(x) = \rho(x) + p^{(i)}_{yy}(x) + p^{(a)}_{yy}(x)$ [there is also the ideal gas contribution $\rho(x)$, which, however, is negligibly small]. As demonstrated in Fig. 3(b), the bulk pressures of the dense and dilute phases are equal. To corroborate that normal and tangential bulk pressures coincide, we also studied walls, which allowed us to directly measure $p_N \simeq p$ as the mechanical pressure exerted onto the walls

[35]. The first insight is, thus, that the swimming pressure of Refs. [19] and [31] is indeed the missing link to define and measure a pressure that is intensive. Looking closer at the interfaces, we see that the pressure difference within the interfaces is unbalanced and, moreover, that p_T is larger than the bulk pressure p. Identifying the interfacial tension with the excess stress (the factor $\frac{1}{2}$ again accounts for the two interfaces) leads to [33]

$$\gamma = \frac{1}{2}\int_0^{L_x} dx[p_N - p_T(x)] \simeq -475, \tag{7}$$

see the inset of Fig. 3(b). The second, quite surprising, insight is that this quantity becomes negative. Our intuition tells us that a system with a negative tension cannot be stable; this is because in systems for which classical thermodynamics is applicable, the interfacial tension determines the excess free energy due to the presence of interfaces. A negative tension implies that the suspension could lower its free energy by creating more interfaces, leading again to a homogeneous state. Quite in contrast, for ABPs one observes a stable, phase-separated state. Another puzzling observation is the magnitude of $|\gamma|$, which is huge compared to typical values ~ 1 in passive liquids (e.g., $\gamma_{\mathrm{LJ}} \simeq 0.42$ has been reported for vapor-liquid coexistence in the Lennard-Jones fluid in two dimensions [44]).

To rationalize a negative tension, we now study the interfacial width w in more detail. Figure 4 shows w obtained from several simulation runs at speed $v_0 = 100$ through fitting Eq. (2). We systematically study different system sizes by holding one box length fixed and varying the other. The total number of particles varies such that the global density is kept constant for all data points. While changing L_x does not influence the width, we observe an increase of w when increasing L_y. This behavior demonstrates two things: First, the system sizes considered here are large enough to have reached a constant width as we vary L_x. Second, the dependance on L_y is compatible with

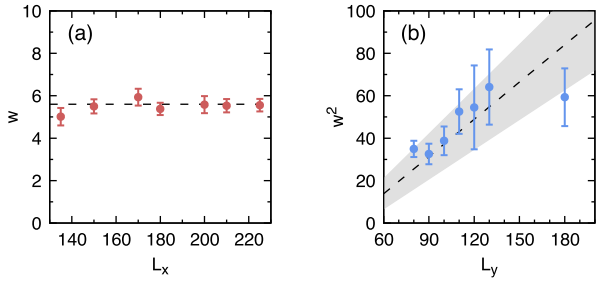

FIG. 4 (color online). Interfacial width w for $v_0 = 100$. (a) As a function of box length L_x for constant $L_y = 90$, where the dashed line indicates $w = 5.6$. (b) As a function of L_y for constant $L_x = 200$. Error bars show the standard deviation of ten independent runs. The dashed line shows the theoretical prediction Eq. (8) with $\kappa \simeq 0.14$. The offset has been adjusted so that $w = 5.6$ for $L_y = 90$ agrees with (a), while the shaded area indicates a conservative error of $\pm 20\%$ in determining γ.

standard capillary wave theory (CWT) assuming equipartition. Hence, it is instructive to recall the arguments leading to CWT [34]: One assumes an ideal instantaneous interface, in our case a line of total length ℓ, that separates the two phases. To change this length, work has to be spent against the positive line tension. Assuming no overhangs, one can decompose the profile $h(y) = \sum_q h_q e^{iqy}$ into Fourier modes h_q. Because the energy for every mode stems from the thermal environment, equipartition implies $\langle |h_q|^2 \rangle = (L_y \kappa q^2)^{-1}$, where κ is the interfacial stiffness governing the fluctuations [45]. For passive liquid-vapor coexistence, this stiffness is related to the tension through $\gamma = k_B T \kappa$ (for the sake of clarity we spell out the thermal energy $k_B T$, which is unity in the employed units).

To estimate the interfacial width w, we calculate the fluctuations of the instantaneous interface [35],

$$w^2 \approx \sum_q \langle |h_q|^2 \rangle = w_0^2 + \frac{L_y}{12\kappa}, \tag{8}$$

which predict a linear divergence due to the capillary waves. The unknown offset w_0^2 corresponds to fluctuations of the $q = 0$ mode, which are bounded due to the periodic boundary conditions. Moreover, we have assumed that equipartition holds even in the driven active suspension, which can be motivated by the fact that orientational degrees of freedom do not develop long-ranged correlations (even in the phase-separated case). While the use of equipartition is of course not rigorous, the predicted leading linear dependence on L_y agrees quite well with the simulation data in Fig. 4(b).

Finally, we argue that stiffness and tension are not independent even in nonequilibrium. The defining paradigm of active matter is the conversion of energy into directed motion. The system (the particles swimming with speed v_0) spends a "housekeeping" work on its environment (typically the solvent) to maintain the steady state far from thermal equilibrium. Within stochastic thermodynamics [46], assuming a hydrodynamic drag $v_0 \mathbf{e}_i$ on the solvent leads to an expression for the work that is consistent with the pressure used here, see [35] for a detailed discussion and derivation. Hence, the work spent by one particle moving a distance ℓ_p is $-v_0 \ell_p$ (in Ref. [27] this expression appears as a positive energy scale). This is the typical energy per particle that is available to the system, in analogy to $k_B T$ being the typical energy that an equilibrium system can "borrow" from the environment. Because this energy determines the magnitude of fluctuations, it suggests the generalization $\gamma = (-v_0 \ell_p)\kappa$ for the interfacial tension of ABPs. With the measured tension γ [Eq. (7)], we find for the stiffness $\kappa \approx \gamma/(-v_0 \ell_p) \simeq 0.14$ for $v_0 = 100$, which is consistent with the measured interfacial widths shown in Fig. 4(b).

In summary, we have demonstrated that the mechanical interfacial tension for phase-separated active Brownian particles is negative. This implies that work is released

when the interfacial length ℓ is increased. However, this work is not "available" to the system, but is part of the work that is spent by the particles to drive the surrounding fluid. We expect that a negative tension is not specific to the model studied here, but holds more generally in active matter. In principle, it can be observed in particle-resolved experiments [10–12] with a stabilized interface. The incorporation of both a negative tension and correct interfacial fluctuations into thermodynamic descriptions based on an effective free energy, a concept that seems to work well for the bulk phases [25,47], is certainly challenging. The reason is that in thermal equilibrium, the same free energy determines the probability of fluctuations away from typical configurations; this connection no longer holds for systems driven away from thermal equilibrium.

We thank Raphael Wittkowski, Jürgen Horbach, Peter Virnau, and Kurt Binder for helpful discussions and comments. We gratefully acknowledge financial support by DFG within priority program SPP 1726 (Grants No. SP 1382/3-1 and No. LO 418/17-1), and ZDV Mainz for computing time on the MOGON supercomputer.

[1] D. Chandler, *Introduction to Modern Statistical Mechanics* (Oxford University Press, Oxford, 1987).
[2] P. Romanczuk, M. Bär, W. Ebeling, B. Lindner, and L. Schimansky-Geier, Eur. Phys. J. Spec. Top. **202**, 1 (2012).
[3] M. C. Marchetti, J. F. Joanny, S. Ramaswamy, T. B. Liverpool, J. Prost, M. Rao, and R. A. Simha, Rev. Mod. Phys. **85**, 1143 (2013).
[4] J. Elgeti, R. G. Winkler, and G. Gompper, Rep. Prog. Phys. **78**, 056601 (2015).
[5] S. Thutupalli, R. Seemann, and S. Herminghaus, New J. Phys. **13**, 073021 (2011).
[6] H. H. Wensink, J. Dunkel, S. Heidenreich, K. Drescher, R. E. Goldstein, H. Löwen, and J. M. Yeomans, Proc. Natl. Acad. Sci. U.S.A. **109**, 14308 (2012).
[7] T. Sanchez, D. T. N. Chen, S. J. DeCamp, M. Heymann, and Z. Dogic, Nature (London) **491**, 431 (2012).
[8] J. Bialké, T. Speck, and H. Löwen, J. Non-Cryst. Solids **407**, 367 (2015).
[9] J. Schwarz-Linek, C. Valeriani, A. Cacciuto, M. E. Cates, D. Marenduzzo, A. N. Morozov, and W. C. K. Poon, Proc. Natl. Acad. Sci. U.S.A. **109**, 4052 (2012).
[10] I. Theurkauff, C. Cottin-Bizonne, J. Palacci, C. Ybert, and L. Bocquet, Phys. Rev. Lett. **108**, 268303 (2012).
[11] J. Palacci, S. Sacanna, A. P. Steinberg, D. J. Pine, and P. M. Chaikin, Science **339**, 936 (2013).
[12] I. Buttinoni, J. Bialké, F. Kümmel, H. Löwen, C. Bechinger, and T. Speck, Phys. Rev. Lett. **110**, 238301 (2013).
[13] J. Bialké, H. Löwen, and T. Speck, Europhys. Lett. **103**, 30008 (2013).
[14] G. S. Redner, M. F. Hagan, and A. Baskaran, Phys. Rev. Lett. **110**, 055701 (2013).
[15] Y. Fily, S. Henkes, and M. C. Marchetti, Soft Matter **10**, 2132 (2014).
[16] J. Stenhammar, A. Tiribocchi, R. J. Allen, D. Marenduzzo, and M. E. Cates, Phys. Rev. Lett. **111**, 145702 (2013).
[17] J. Stenhammar, D. Marenduzzo, R. J. Allen, and M. E. Cates, Soft Matter **10**, 1489 (2014).
[18] A. Wysocki, R. G. Winkler, and G. Gompper, Europhys. Lett. **105**, 48004 (2014).
[19] S. C. Takatori, W. Yan, and J. F. Brady, Phys. Rev. Lett. **113**, 028103 (2014).
[20] I. Llopis and I. Pagonabarraga, Europhys. Lett. **75**, 999 (2006).
[21] T. Ishikawa and T. J. Pedley, Phys. Rev. Lett. **100**, 088103 (2008).
[22] A. Zöttl and H. Stark, Phys. Rev. Lett. **112**, 118101 (2014).
[23] J. Tailleur and M. E. Cates, Phys. Rev. Lett. **100**, 218103 (2008).
[24] T. Speck, J. Bialké, A. M. Menzel, and H. Löwen, Phys. Rev. Lett. **112**, 218304 (2014).
[25] M. E. Cates and J. Tailleur, Annu. Rev. Condens. Matter Phys. **6**, 219 (2015).
[26] R. Wittkowski, A. Tiribocchi, J. Stenhammar, R. J. Allen, D. Marenduzzo, and M. E. Cates, Nat. Commun. **5**, 4351 (2014).
[27] S. C. Takatori and J. F. Brady, Soft Matter **10**, 9433 (2014).
[28] F. Ginot, I. Theurkauff, D. Levis, C. Ybert, L. Bocquet, L. Berthier, and C. Cottin-Bizonne, Phys. Rev. X **5**, 011004 (2015).
[29] S. K. Das, S. A. Egorov, B. Trefz, P. Virnau, and K. Binder, Phys. Rev. Lett. **112**, 198301 (2014).
[30] A. P. Solon, Y. Fily, A. Baskaran, M. E. Cates, Y. Kafri, M. Kardar, and J. Tailleur, Nat. Phys. (to be published).
[31] X. Yang, M. L. Manning, and M. C. Marchetti, Soft Matter **10**, 6477 (2014).
[32] F. Schmitz, P. Virnau, and K. Binder, Phys. Rev. E **90**, 012128 (2014).
[33] J. G. Kirkwood and F. P. Buff, J. Chem. Phys. **17**, 338 (1949).
[34] R. Evans, Adv. Phys. **28**, 143 (1979).
[35] See Supplemental Material at http://link.aps.org/supplemental/10.1103/PhysRevLett.115.098301 for details on the numerical methods, numerical results in the presence of walls, and derivations of Eqs. (6), (7), and (8), which includes Refs. [36–39].
[36] J. D. Weeks, D. Chandler, and H. C. Andersen, J. Chem. Phys. **54**, 5237 (1971).
[37] T. Speck, A. M. Menzel, J. Bialké, and H. Löwen, J. Chem. Phys. **142**, 224109 (2015).
[38] P. J. Steinhardt, D. R. Nelson, and M. Ronchetti, Phys. Rev. B **28**, 784 (1983).
[39] T. Speck, J. Mehl, and U. Seifert, Phys. Rev. Lett. **100**, 178302 (2008).
[40] M. Schrader, P. Virnau, and K. Binder, Phys. Rev. E **79**, 061104 (2009).
[41] J. A. Barker and D. Henderson, J. Chem. Phys. **47**, 4714 (1967).
[42] J. Walton, D. Tildesley, J. Rowlinson, and J. Henderson, Mol. Phys. **48**, 1357 (1983).
[43] A. P. Solon, J. Stenhammar, R. Wittkowski, M. Kardar, Y. Kafri, M. E. Cates, and J. Tailleur, Phys. Rev. Lett. **114**, 198301 (2015).
[44] M. Santra, S. Chakrabarty, and B. Bagchi, J. Chem. Phys. **129**, 234704 (2008).
[45] Conventionally, stiffness and tension have the same units. For our purposes, however, it is more transparent to introduce a modified stiffness κ as an inverse length.
[46] U. Seifert, Rep. Prog. Phys. **75**, 126001 (2012).
[47] S. C. Takatori and J. F. Brady, Phys. Rev. E **91**, 032117 (2015).